https://doi.org/10.5194/acp-2021-951
Preprint. Discussion started: 15 December 2021

Atmospheric Chemistry and Physics Discussions

Functionality-Based Formation of Secondary Organic Aerosol from *m*-Xylene Photooxidation

Yixin Li[1,2], Jiayun Zhao[1], Mario Gomez-Hernandez[1], and Renyi Zhang[1,3*]

[1]Department of Chemistry, Texas A&M University, College Station, TX 77843, USA

[2]Department of Chemistry, University of California Irvine, Irvine, CA 92697, USA

[3]Department of Atmospheric Sciences, Texas A&M University, College Station, TX 77843, USA

ABSTRACT. Photooxidation of volatile organic compounds (VOCs) produces condensable oxidized organics (COOs) to yield secondary organic aerosol (SOA), but the fundamental chemical mechanism for gas-to-particle conversion remains uncertain. Here we elucidate the production of COOs and their roles in SOA and brown carbon (BrC) formation from *m*-xylene oxidation by simultaneous monitoring the evolutions of gas-phase products and aerosol properties in an environmental chamber. Four COO types with the distinct functionalities of dicarbonyls, carboxylic acids, polyhydroxy aromatics/quinones, and nitrophenols are identified from early-generation oxidation, with the yields of 25%, 37%, 5%, and 3%, respectively. SOA formation occurs via several heterogeneous processes, including interfacial interaction, ionic dissociation/acid-base reaction, and oligomerization, with the yields of (20 ± 4)% and (32 ± 7)% at 10% and 70% relative humidity (RH), respectively. Chemical speciation shows the dominant presence of oligomers, nitrogen-containing organics, and carboxylates at RH and carboxylates at low RH. The identified BrC includes N-heterocycles/N-heterochains and nitrophenols, as evident from reduced single scattering albedo. The measured uptake coefficient (γ) for COOs is dependent on the functionality, ranging from 3.7×10^{-4} to 1.3×10^{-2}. A kinetic framework is developed to predict SOA production from the concentrations and uptake coefficients for COOs. This functionality-based approach well reproduces SOA formation from *m*-xylene oxidation and is broadly applicable to VOC oxidation for other species. Our results reveal that photochemical oxidation of *m*-xylene represents a major source for SOA and BrC formation under urban environments, because of its large abundance, high reactivity with OH, and high yields for COOs.

Corresponding to: Email: renyi-zhang@tamu.edu

https://doi.org/10.5194/acp-2021-951
Preprint. Discussion started: 15 December 2021

Atmospheric Chemistry and Physics Discussions

1. Introduction

Photooxidation of anthropogenic and biogenic volatile organic compounds (VOCs) produces tropospheric ozone and secondary organic aerosol (SOA), with profound implications for air quality, human health, and climate (Pope et al., 2002; Li et al., 2007; IPCC, 2013; NASEM, 2016; Zhu et al., 2017; Molina, 2021; Zhang et al., 2021). VOC oxidation is initiated by various oxidants (e.g., OH, O_3, NO_3, etc.) and proceeds via multiple pathways and stages (Atkinson, 2000; Suh et al., 2001; Zhang et al., 2002; Zhao et al., 2004; Wennberg et al., 2018), yielding condensable oxidized organics (COOs) to form SOA and brown carbon (BrC) via gas-to-particle conversion (Finlayson-Pitts and Pitts, 2000; Moise et al., 2015; Seinfeld and Pandis, 2016). The enormous chemical complexity for VOC oxidation and gas-to-particle conversion represents one of the greatest challenges in atmospheric chemistry research (Ravishankara, 1997; Zhang et al., 2015; NASEM, 2016). Aromatic hydrocarbons (e.g., benzene, toluene, xylenes, and trimethylbenzene) account for 20-30% of the total VOCs and are the major anthropogenic SOA precursors in the urban atmosphere (Calvert et al., 2002; Ng et al., 2007; Song et al., 2007; Guo et al., 2014; Seinfeld and Pandis, 2016). For example, *m*-xylene or $C_6H_4(CH_3)_2$ represents an important type of aromatic hydrocarbons, which is emitted primarily from industrial and traffic sources. The concentration of *m*-xylene ranges in a level from sub part per billion (ppb) up to several tens of ppb under urban environments (Calvert et al., 2002; Fortner et al., 2009). Photooxidation of *m*-xylene is primarily initiated by OH with a rate constant of 2.4×10^{-11} cm^3 $molecule^{-1}$ s^{-1}, which is nearly four times higher than that of toluene (Fan and Zhang, 2008; Ji et al., 2017). The OH-*m*-xylene reactions occur via dominantly OH-addition to the aromatic ring to yield *m*-xylene-OH adducts and minorly H-abstraction from the methyl group to form methylbenzyl radicals (about 4%) (Fan and Zhang, 2008). The *m*-xylene-OH adducts then react with O_2 to form dimethylphenol via H-extraction or OH-*m*-

https://doi.org/10.5194/acp-2021-951
Preprint. Discussion started: 15 December 2021


Atmospheric Chemistry and Physics Discussions

xylene-O_2 peroxy radicals (RO_2) via O_2 addition. A laboratory study identified *m*-tolualdehyde, *m*-dimethylphenols, and dicarbonyls (i.e., glyoxal, methylglyoxal, unsaturated dicarbonyls, and epoxy carbonyls) as the main gas-phase products from OH-initiated oxidation of *m*-xylene (Zhao et al., 2005).

Several types of condensable oxidized organics (COOs) with distinct functionality and volatility are produced form *m*-xylene photooxidation. SOA formation is conventionally considered to be mainly resulted from equilibrium gas-particle partitioning of semi-, intermediate-, or low-volatile products (Shrivastava et al., 2017). Aromatic oxidation by OH yields low-volatile polyhydroxy aromatics/quinones (denoted as PAQ hereafter), which condense to the aerosol-phase (Schwantes et al., 2017). Also, chain autoxidation reactions of RO_2 from aromatics photooxidation likely yield highly oxygenated molecules (HOMs) with low volatility (Molteni et al., 2018; Garmash et al., 2020; Wang et al., 2020), although the reported yield of HOMs from *m*-xylene oxidation is small (1.0% to 1.7%) (Molteni et al., 2018). Several key oxidation products of aromatic oxidation have been shown to readily engage in multiphase reactions and contribute to SOA formation (Ji et al., 2020, Li et al., 2021a). A recent experimental study demonstrated that SOA formation from toluene photooxidation is mainly contributed by volatile dicarbonyls and organic acids (Li et al., 2021b). Moreover, the aqueous reactions between small α-dicarbonyls and base species (e.g., ammonia and amines) produce light-absorbing brown carbon (BrC) (De Haan et al., 2011, 2017; Marrero-Ortiz et al., 2019; Li et al., 2021a,b). Previous experimental studies identified the presence of hydroxy (C-OH), carbonyl (C=O), and acetal (C-O-C) bonds as the main functional groups in aromatic-derived SOA formed via aqueous reactions, implicating a role of oxygenated organics in SOA formation (Jia and Xu, 2014; Jia and Xu, 2018; Zhang et al., 2019). Also, laboratory

https://doi.org/10.5194/acp-2021-951
Preprint. Discussion started: 15 December 2021


Atmospheric Chemistry and Physics Discussions

experiments showed that coating of *m*-xylene SOA on black carbon particles significantly enhances scattering, absorption, and single scattering albedo (SSA) (Guo et al., 2016).

Current atmospheric models mainly parameterize SOA formation based on equilibrium partitioning for semi- to low-volatile COOs (Shrivastava et al., 2017). However, gas-to-particle conversion corresponds to decreasing entropy (i.e., $\Delta S \ll 0$), represents non-equilibrium chemical processes (Peng et al., 2021). Moreover, the occurrence of particle-phase reactions significantly alters the physiochemical properties (including volatility, hygroscopicity, and optical properties) for COOs (Tan et al., 2012; Faust et al., 2017; Ji et al., 2020; Li et al., 2021a,b; Liu et al., 2021). Notably, the volatility-based approach consistently under-predicts SOA formation (Heald et al., 2005; Zhang et al., 2015; Hodzic et al., 2016), particularly during haze formation under polluted conditions (Guo et al., 2014; Peng et al., 2021). Here we investigate the production of COOs with different functionalities and assess their roles in SOA formation from *m*-xylene oxidation. A primary objective of this work is to establish a functionality-based framework to predict SOA formation from VOC photooxidation.

2. Experimental Methodology

The production of COOs and their roles in SOA formation from *m*-xylene oxidation were investigated using an environmental chamber (See Method and Figure S1 in the Supplementary Information or SI), similar to our previous studies (Li et al., 2021a,b). Briefly, monodispersed sub-micrometer seed particles were exposed to *m*-xylene-OH oxidation products, and the evolutions of the gaseous products and aerosol properties were simultaneously measured. The time-dependent gaseous concentrations of *m*-xylene and its oxidation products were detected using an ion drift - chemical ionization mass spectrometry (Fotner et al., 2014). The temporally resolved particle size, number concentration, SSA, and density were measured using an integrated aerosol system

https://doi.org/10.5194/acp-2021-951
Preprint. Discussion started: 15 December 2021


Atmospheric Chemistry and Physics Discussions

consisting of a differential mobility analyzer, a condensation particle counter, an integrating nephelometer, a cavity ring-down spectrometer, and an aerosol particle mass analyzer (Zhang et al., 2020; Li et al., 2021b). The size evolution was quantified by a growth factor (GF), which is defined by D_p/D_0, where D_p is the diameter after the exposure to *m*-xylene oxidation and D_0 = 100 nm is the initial diameter. In addition, chemical composition was analyzed after seed particles were exposed to *m*-xylene oxidation for 20 mins and collected for 2 additional hours by a thermal desorption - ion drift - chemical ionization mass spectrometer (TD-ID-CIMS) (Zhang et al., 2009). All measured particle properties were relevant to dry conditions (i.e., less than 5% RH) (Li et al., 2021b).

Three types of seed particles were produced to represent various chemical compositions, i.e., NH_4HSO_4 - ammonium bisulfate (ABS), $(NH_4)_2SO_4$ - ammonium sulfate (AS) in the presence and absence of NH_3, and NaCl - sodium chloride. Measurements of SOA/BrC formation were also conducted by varying RH, NH_3, and NO_x (= NO and NO_2). An uptake coefficient (γ) for COOs was derived from the measured size growth of particles and the corresponding gas-phase concentrations. In addition, we simulated the time-dependent production of the gaseous products by employing a tri-exponential kinetic model to account for the gas-phase oxidation, chamber wall loss, and aerosol uptake. The major advantages of our analytical methodologies lied in simultaneous monitoring of the evolutions of gaseous oxidation products and aerosol properties when seed particles were exposed to the oxidation products. Specifically, our experimental approach remedied the deficiency of wall loss of reactive gaseous and particles, which represents a main obstacle in experimental investigation using environmental chambers (Zhang et al., 2014; Huang et al., 2018). In addition, our analytical approach provided detailed chemical speciation without inducing fragmentation and allowed for differentiation of the contributions of multi-

https://doi.org/10.5194/acp-2021-951
Preprint. Discussion started: 15 December 2021


Atmospheric Chemistry and Physics Discussions

generation products to SOA formation (Li et al., 2021b). By categorizing COOs in accordance with the functional groups, we establish a framework to predict SOA formation from the measured production and reactivity.

3. Results and Discussions

3.1 Evolution of oxidation products

To elucidate the production of COOs, we measured time-dependent gaseous concentrations of *m*-xylene oxidation products. While the *m*-xylene mixing ratio exhibits an exponential decay throughout the experiments (Figure 1a), the formation of the gas-phase oxidation products follows the rate-determining steps involving successive OH-oxidation with three major generations (Figure 1b-e). The first-generation products (P_1) include dimeththylphenol (*m/z* = 123) and methylbenzaldehyde (*m/z* = 121), corresponding to OH addition to the aromatic ring (~96%) and hydrogen extraction (~4%) from the methyl group, respectively (Fan and Zhang, 2008; Li et al., 2021b). The second-generation products (P_2) mainly consist of methylglyoxal (*m/z* = 73), methylbutenedial (*m/z* = 99), toluic acid (*m/z* = 137), and dimethylresorcinol (Figure 1f and Figure S2), which are produced from the P_1 reactions with OH/HO_2. For example, methylglyoxal and methylbutenedial are formed from OH oxidation of dimeththylphenol and subsequent ring-opening or from the primary peroxy radical. The latter undergoes cyclization to form the bicyclic radical, which then reacts with O_2 to form the secondary peroxy radical, followed by reactions with HO_2 and subsequent ring-cleavage (Fan and Zhang, 2008). The third-generation products (P_3) contain mainly multi-functional organic acids, including pyruvic acid (*m/z* = 89), 4-oxo-2-pentenoic acid (*m/z* = 115), and 3-methyl-4-oxo-2-pentenoic acid (*m/z* = 129) produced from the subsequent reactions of dicarbonyls with OH.

https://doi.org/10.5194/acp-2021-951
Preprint. Discussion started: 15 December 2021


Atmospheric Chemistry and Physics Discussions

144 The P_1 concentrations rise immediately upon initiating photooxidation and reach the peak
145 mixing ratios of about 20 ppb for dimeththylphenol and 9 ppb for methylbenzaldehyde. There is a
146 slight decline in P_1 concentrations after 70 to 100 mins, reflecting their consumption from further
147 OH oxidation (Figure 1c). The P_2 concentrations follow those of P_1 (Figure 1d and Figure S3a)
148 and reach the peak mixing ratios ranging from 0.4 to 2.4 ppb, dependent on their subsequent
149 oxidation by OH as well as loss to the chamber wall and aerosols. Note that the concentration of
150 toluic acid rises later than those of the dicarbonyls, attributable to the slower rates for H-abstraction
151 by OH from the methyl group than OH-addition to the aromatic ring (Fan and Zhang, 2008). The P_3
152 concentrations increase monotonically after a delay of 10-20 mins and reach a mixing ratio from
153 sub-ppb to 2.5 ppb at 120 min (Figure 1e and Figure S3b). The initial concentration of *m*-xylene
154 (e.g., 1940 ppb) in our experiment is higher than that in the atmosphere, potentially inducing self-
155 and cross-reactions of RO_2 to form alkoxy radicals (RO) or dialkyl peroxides (ROOR') leading to
156 HOMs. However, negligible products relevant to HOMs were detected in our experiments,
157 indicating a minor importance for the self- and cross-reactions of RO_2 compared to the competing
158 reactions between RO_2 and HO_2/NO/RO_2 to form ring-opening products.

159 We simulated the time-dependent evolution of the gaseous products by employing a tri-
160 exponential kinetic model (Figure 1b and Table S1). Multi-generation oxidation of *m*-xylene
161 occurs via consecutive reaction steps to produce a multi-generation product, P_n (where *n* denotes
162 the sequence of OH oxidation), which subsequently engages in additional OH oxidation, wall loss,
163 and aerosol loss. Figure 1b-d indicates that the simulated concentrations well reproduce those
164 measured for P_1 to P_3 by adopting our measured γ (to be discussed below) and estimated wall loss
165 rates (see Methods and Table S1 in SI).

166 **3.2 Particle size growth, SSA, and chemical speciation**

https://doi.org/10.5194/acp-2021-951
Preprint. Discussion started: 15 December 2021


Atmospheric Chemistry and Physics Discussions

To evaluate SOA and BrC formation from COOs, we measured the time-dependent GF, SSA, and density, after $(NH_4)_2SO_4$ seed particles are exposed to the *m*-xylene oxidation products in the presence of 19 ppb NH_3 and at 70% RH (Figure 2a-c). The GF increases monotonically and reaches a value of (2.41 ± 0.03) at 120 min (Figure 2a), while the SSA declines steadily throughout the exposure and reaches the value of (0.91 ± 0.01) at 120 min (Figure 2b). The latter is indicative of the production of light-absorbing BrC. The measured SSA for *m*-xylene is lower than that previously reported for toluene under comparable experimental conditions (Li et al., 2021b). The difference in SSA/BrC formation between toluene and *m*-xylene is explained by a higher yield of methylglyoxal from *m*-xylene than from toluene (Jenkin et al., 2003; Nishino et al., 2010), since methylglyoxal produces BrC more efficiently via aqueous reaction than glyoxal (Li et al., 2021a). Analysis of particle chemical composition using thermal desorption - ion drift - chemical ionization mass spectrometer (TD-ID-CIMS) reveals high abundances of oligomers, nitrogen-containing organics (NCO) consisting of N-heterocycles/N-heterochains, carboxylates, along with a small amount of dimethylresorcinol/benzoquinone (Figure 2c). The identified mass peaks are summarized in Tables S2 to S4. Assuming similar sensitivity to proton-transfer reactions for the aerosol-phase organics, i.e., with the proton transfer reaction rate constants of (2 to 4) × 10^{-9} cm^3 $molecule^{-1}$ s^{-1} (Zhao and Zhang, 2004), the contributions of oligomers, NCO, carboxylates, and dimethylresorcinol/benzoquinone to the total SOA formation are estimated to be 22%, 23%, 47%, and 8%, respectively, at 70% RH (Table S5). Note that the TD-ID-CIMS method preserves the identify for all organic species without fragmentation, providing unambiguous chemical speciation for the aerosol-phase products.

3.3 Effects of seed particles, RH, and NH_3, and NOx

https://doi.org/10.5194/acp-2021-951
Preprint. Discussion started: 15 December 2021


Atmospheric Chemistry and Physics Discussions

We assessed the dependence of SOA/BrC formation from *m*-xylene-OH oxidation on different seed particles, concentrations of NH_3/NO_x, and RH. Figure 3a shows that $(NH_4)_2SO_4$ in the presence of 19 ppb NH_3 exhibits the largest GF and lowest SSA at 120 min, which are explained by the chemical mechanisms leading to the formation of the observed aerosol-phase products. While dicarbonyls undergo aqueous phase reactions to form oligomers (Figure S4) (Ji et al., 2020; Li et al., 2021a), organic acids engage in ionic dissociation and acid-base reaction to yield carboxylates (Figure 3b). In addition, the reaction of dicarbonyls with NH_3 produce N-heterocycles/N-heterochains (Figure S5), which are light-absorbing (Marrero-Ortiz et al., 2019; Li et al., 2021a). Oligomerization of dicarbonyls involves protonation, hydration, and deprotonation, which are mediated by carbenium ions via nucleophilic addition (Ji et al., 2020; Li et al., 2021a). While protonation of dicarbonyls to yield carbenium ions is promoted by hydrogen ion activity, high acidity hinders hydration and deprotonation, explaining the largest GF and the smallest SSA on weakly acidic $(NH_4)_2SO_4$ particles in the presence NH_3 (Figure 3a). In addition, uptake of dicarbonyls, organic acids, and PAQ is likely facilitated on aqueous $(NH_4)_2SO_4$ particles, because of surface propensity of charge-separation at the interface (Hua et al., 2011; Shi et al., 2020). Specifically, surface-abundant NH_4^+ cations arising from interfacial charge separation of $(NH_4)_2SO_4$ likely exert electrostatic attraction to gaseous oxygenated species (with a negative charge character) to enhance uptake for dicarbonyls, organic acids, and PAQ (Li et al., 2021a,b). The most efficient formation of SOA and BrC on $(NH_4)_2SO_4$ particles in the presence of NH_3 are also consistent with the measured highest intensities for oligomers and NCO (Figure 3b). On the other hand, ionic dissociation and acid-base reaction to yield carboxylates occur efficiently in the presence of NH_3/NaCl, as evident from the increasing carboxylate intensity from NH_4HSO_4 to NaCl (Figure 3b). The GF and SSA increase and decrease, respectively, with NH_3 from 0 to 27

https://doi.org/10.5194/acp-2021-951
Preprint. Discussion started: 15 December 2021


Atmospheric Chemistry and Physics Discussions

ppb for all three types of seed particles (Figure 4a,b), relevant to the reactions of NH_3 with dicarbonyls to form NCO and with organic acids to form ammonium carboxylates. The analysis of the particle composition confirms that the intensities of oligomers, NCO, and carboxylates increase with the NH_3 concentration (Figure 4c-e).

We carried out additional experiments by varying RH from 10% to 70% in the presence of 19 ppb NH_3 (Figure 5). The GF decreases with increasing RH from (3.10 ± 0.06) at RH = 10% to (2.41 ± 0.03) at RH = 70% (Figure 5a). The measured SSA at 120 min is close to unity at 10% and 30% RH and decreases with increasing RH (Figure 5a), indicating negligible NCO formation at low RH but significant NCO formation at RH above 50%. Carboxylates represent the dominant constituent throughout the RH range (i.e., 85% at 10% RH to 47% at 70% RH), while the contributions of oligomers and NCO are small at low RH (2-5% at RH < 40%) and become increasingly significant at high RH (15-23% at RH > 50%) (Figure 5b). The fraction for PAQ (8%) is nearly invariant with RH. For $(NH_4)_2SO_4$ particles, the deliquescent and efflorescent points are at 80% and 36% RH, respectively (Li et al., 2021b). At low RH (10% and 30%), aqueous reactions to yield oligomers/NCO are minimal because of small water activity and significantly suppressed protonation and oligomerization. On the other hand, carboxylic acids readily undergo ionic dissociation or acid-base reaction, since organic acids efficiently retain water even at low RH (Xue, 2009). The equilibrium vapor pressures for PAQ are much lower than those for organic acids (Table S6), facilitating more efficient condensation. Additionally, wall-loss of COOs is more pronounced at high RH (Li et al., 2021b), explaining the decreased GF with increasing RH. Measurement of gaseous concentrations for COOs shows that wall-loss is 1.5 to 4.6 times more efficient at 70% RH than at 10% RH, while wall loss of *m*-xylene is negligible at both RH levels (Table S7).

https://doi.org/10.5194/acp-2021-951
Preprint. Discussion started: 15 December 2021


Atmospheric Chemistry and Physics Discussions

We determined the total density and the density of the SOA fraction for $(NH_4)_2SO_4$ seed particles exposed to *m*-xylene oxidation (Figure 5 c,d). The measured densities are distinct between 10 and 70% RH. At 10% RH, the total density decreases monotonically, while the SOA density increases slightly with reaction time, i.e., from 1.27 to 1.39 g cm^{-3} (Figure 5c), indicating minor oligomers and dominant carboxylic acids at low RH. At 70% RH, the total particle density initially decreases from 1.77 g cm^{-3} to 1.41 g cm^{-3} (at a GF of 1.24) and subsequently increases steadily to 1.56 g cm^{-3} at 120 min. The SOA density on $(NH_4)_2SO_4$ particles increases from 1.26 g cm^{-3} at 10 min to 1.55 g cm^{-3} at 120 min (Figure 5d). The evolution in the densities reflects the variation in the chemical composition. The initial particle growth is dominated by small oligomers, imidazoles from methylglyoxal/methylbutenedial, and early-generation organic acids (e.g., toluic acid), with the densities from 0.98 to 1.27 g cm^{-3} (Table S8). Subsequent particle growth from methylglyoxal/methylbutenedial yields large oligomers, with the densities of 1.71-1.90 g cm^{-3} (Table S8).

To evaluate the NO_x effects, we performed experiments on $(NH_4)_2SO_4$ seed particles by varying the initial NO_x concentration from 0 to 500 ppb (Figure 6). Three major nitrophenols are identified from NO_2 addition to the OH-*m*-xylene adduct, i.e., 4-methyl-2-nitrophenol (*m/z* = 154), dimethyl nitrophenol (*m/z* = 168), and dimethyl-4-nitrocatechol (*m/z* = 184) (Figure 6a). The production of nitrophenols is much smaller than those for dicarbonyls and organic acids, consistent with a smaller yield (less than 7%) for nitrophenols (Fan and Zhang, 2008). The GF on $(NH_4)_2SO_4$ seed particles with NH_3 decreases from 2.41 ± 0.03 to 2.18 ± 0.03 with 0 to 500 ppb NO_x (Figure 6b). The SSA decreases significantly from 0.911 ± 0.006 to 0.839 ± 0.003 with increasing NO_x (Figure 6b), because of the formation of light-absorbing nitrophenols (Hems and Abbatt, 2018; Li et al., 2021b). Analysis of particle composition reveals that the decreasing GF with increasing NO_x

https://doi.org/10.5194/acp-2021-951
Preprint. Discussion started: 15 December 2021


Atmospheric Chemistry and Physics Discussions

257 correlates with simultaneous decreases of carboxylates, oligomers, and NCOs and with increasing
258 nitrophenols in the aerosol-phase (Figure 6c). Overall, nitrophenols contribute 2% to 4% to the
259 SOA formation. Addition of NO_x does not only produce nitrophenols and but also alters the cycling
260 between RO_2 and alkoxy (RO) radicals, leading to re-distributions of COOs. The presence of NO_x
261 decreases dicarbonyls and organic acids, as evident from decreased intensities for oligomers, NCO,
262 and carboxylates in the aerosol-phase with increasing NO_x (Figure 2h).

263 **3.4 COO and SOA Yields**

264 From the measured GF and COO concentrations, we derived the γ, which is widely
265 employed to represent aerosol formation in atmospheric models (Zhang et al., 2015). The measured
266 γ varies with the functionality of COOs and RH on $(NH_4)_2SO_4$ seed particles (Figure 7a). Results
267 of the γ values for COOs are also summarized in Table S9. The γ for dicarbonyls is the highest
268 (from 3×10^{-3} to 1.3×10^{-2}) at 70% RH but is significantly reduced (from 3.7×10^{-4} to 1.0×10^{-3})
269 at 10% RH, while the γ's for organic acids, PAO, and nitrophenols are slightly higher at 70% RH.
270 Among the organic acids, the γ correlates with the acid dissociation constant and solubility, which
271 are the highest for pyruvic acid and the lowest for toluic acid. The standard variation in γ (within
272 one σ) among each COO type is within 50%, 40%, 30%, and 15% for dicarbonyls, organic acids,
273 PAO, and nitrophenols, respectively. From the measured concentrations of COOs and *m*-xylene,
274 we determined the COO yields (Y_{COO}),

275 $$Y_{COO} = [COO_i]/\Delta[C_6H_4(CH_3)_2] \quad (1)$$

276 where *i* represents the type of COO species (i.e., dicarbonyls for $i = 1$, carboxylic acids for $i = 2$,
277 PAO for $i = 3$, and nitrophenols for $i = 4$), $[COO_i]$ denotes the concentration of COO species *i* with
278 correction for wall-loss (see SI Methods), and $\Delta[C_6H_4(CH_3)_2]$ is the concentration of *m*-xylene
279 consumed due to OH oxidation. The Y_{COO} values for dicarbonyls, organic acids, PAO, and

https://doi.org/10.5194/acp-2021-951
Preprint. Discussion started: 15 December 2021


Atmospheric Chemistry and Physics Discussions

nitrophenols are 25%, 37%, 5%, and 3%, respectively (Figure 7b), indicating significant production of COOs from *m*-xylene oxidation.

Hence, our results show that gas-to-particle conversion from *m*-xylene oxidation involves several distinct heterogeneous processes, including interfacial attraction, ionic dissociation/acid-base reaction, and nucleophilic oligomerization, which cannot be described by equilibrium partitioning. We established a functionality-based SOA formation to predict the aerosol mass concentration (M_{SOA}) from the measured gaseous concentrations and γ's for COOs,

$$M_{SOA} = \sum_i \frac{1}{4} \gamma_i C_i S[COO_i] MW_i \quad (2)$$

where C_i is the thermal velocity for species i, S is the available particle surface area per unit volume, and MW_i is the molar weight for species i. The M_{SOA} is calculated using the averaged γ (Figure 3c and Table S10) and the measured time-averaged concentrations for each COO type (Table S7). While the production of COOs is dependent on the VOC types and photooxidation, the aerosol-phase reactivity of COOs, as represented by γ, is only dependent on the functionality for a given aerosol type. Thus, SOA formation from various VOC types can be predicted from the production and reactivity for COOs based on the experimental measurements, by categorizing COOs in accordance with their functional groups.

To assess the consistency of this approach, we compared the predicted and measured SOA mass yields (Y_{SOA}),

$$Y_{SOA} = M_{SOA}/(\Delta[C_6H_4(CH_3)_2] \times MW_m) \quad (3)$$

where MW_m is the molar weight of *m*-xylene. The predicted Y_{SOA} is (11 ± 3)% and (6 ± 1)%, respectively, at 10% and 70 % RH, comparable to the measured values of (14 ± 0.4)% and (6.3 ± 0.2)% on $(NH_4)_2SO_4$ seed particles (Figure 7c). The slight differences between the predicted and measured Y_{SOA}'s are explainable by the uncertainties related to lumping each COO type (i.e.,

https://doi.org/10.5194/acp-2021-951
Preprint. Discussion started: 15 December 2021


Atmospheric Chemistry and Physics Discussions

303 averaging the γ values) as well as unaccounted low-abundant COO species. To account for the
304 RH-dependent wall loss for COOs, we corrected Y_{SOA} from the measured gaseous concentrations
305 at varying RH (see Methods and Table S7). Such correction results in an increase of about one to
306 four times for Y_{SOA} at 10% and 70% RH, yielding the values of (20 ± 4)% and (32 ± 7)%,
307 respectively (Figure 7c). Under atmospheric conditions, SOA/BrC formation from *m*-xylene is
308 expected to be enhanced at high RH, because of significantly enhanced aqueous reaction, larger
309 aerosol surface-area, and higher water activity. Field measurements showed significantly enhanced
310 SOA formation with increasing RH during severe haze evolution (Guo et al., 2014; Peng et al., 2021).

311 **4. Conclusions**

312 In this work we have elucidated the production of COOs and assess their roles in SOA
313 formation from *m*-xylene oxidation. OH-initiated oxidation of *m*-xylene produces four distinct
314 COO types consisting of dicarbonyls, carboxylic acids, polyhydroxy aromatics/quinones, and
315 nitrophenols from early-generation (P_2 and P_3), with the yields of 25%, 37%, 5%, and 3%,
316 respectively. SOA formation occurs via several heterogeneous processes, including interfacial
317 interaction, ionic dissociation/acid-base reaction, and oligomerization, with the yields of (20 ± 4)%
318 at 10% RH and (32 ± 7)% at 70% RH. The identified aerosol-phase products include dominant
319 oligomers, N-heterocycles/N-heterochains, and carboxylates at high RH and dominant
320 carboxylates at low RH, along with small amounts of PAQ and nitrophenols (in the presence of
321 NO_x). The nitrogen-containing organics consisting of N-heterocycles, N-heterochains, and
322 nitrophenols are light-absorbing, characterized by low SSA. The measured γ for COOs is
323 dependent on the functionality, ranging from 3.7×10^{-4} to 1.3×10^{-2}. A kinetic framework is
324 developed to predict SOA formation from the concentration and γ for COOs. Our results illustrate
325 that SOA formation from *m*-xylene oxidation is accurately quantified from the abundance and

https://doi.org/10.5194/acp-2021-951
Preprint. Discussion started: 15 December 2021


Atmospheric Chemistry and Physics Discussions

reactivity for COOs (i.e., eq. 2). Notably, this kinetic framework accounts for the interfacial process (i.e., mass accommodation) as well as aqueous reactions (i.e., oligomerization and acid-base reactions) without the assumption of gas-particle equilibrium. We envisage that this functionality-based approach is broadly applicable to predict SOA formation from VOC photooxidation using experiment/field measured or model-simulated COOs, aerosol surface area, and reactivity. We conclude that photochemical oxidation of *m*-xylene represents a major source for SOA and BrC formation under urban conditions, because of its large abundance, high reactivity with OH, and high yields for COOs.

ACKNOWLEDGEMENTS

This research was supported by the Robert A. Welch Foundation (Grant A-1417). Y.L. was supported by a dissertation Fellowship at Texas A&M University.

https://doi.org/10.5194/acp-2021-951
Preprint. Discussion started: 15 December 2021

Atmospheric Chemistry and Physics Discussions

REFERENCES

Atkinson, R. Atmospheric Chemistry of VOCs and NO_x. Atmos. Environ., 34, 2063–2101, 2000.

Calvert, J. G., Atkinson, R., Becker, K. H., Kamens, R. M., Seinfeld, J. H., Wallington, T. H., and Yarwood, G.: The Mechanisms of Atmospheric Oxidation of Aromatic Hydrocarbons, Oxford University Press: New York., 2002.

Fan, J., and Zhang, R.: Density Functional Theory Study on OH-Initiated Atmospheric Oxidation of m-Xylene, J. Phys. Chem. A, 112(18), 4314–4323, doi:10.1021/jp077648j, 2008.

Finlayson-Pitts, B. J., and Pitts, J. N.: Chemistry of the Upper and Lower Atmosphere: Theory, Experiments and Applications, Academic Press, San Diego, 2000.

Faust, J. A., Wong, J. P. S., Lee, A. K. Y., and Abbatt, J. P. D.: Role of Aerosol Liquid Water in Secondary Organic Aerosol Formation from Volatile Organic Compounds, Environ. Sci. Technol., 51, 1405− 1413, 2017.

Fortner, E. C., Zheng, J., Zhang, R., Berk Knighton, W., Volkamer, R. M., Sheehy, P., Molina, L., and André, M.: Measurements of Volatile Organic Compounds Using Proton Transfer Reaction – Mass Spectrometry during the MILAGRO 2006 Campaign, Atmos. Chem. Phys., 9(2), 467–481, doi:10.5194/acp-9-467-2009, 2009.

Fortner, E.C., Zhao, J., and Zhang, R.: Development of ion drift-chemical ionization mass spectrometry, Anal. Chem., 76, 5436-5440, 2004.

Garmash, O., Rissanen, M. P., Pullinen, I., Schmitt, S., Kausiala, O., Tillmann, R., Zhao, D., Percival, C., Bannan, T. J., Priestley, M., Hallquist, Å. M., Kleist, E., Kiendler-Scharr, A., Hallquist, M., Berndt, T., McFiggans, G., Wildt, J., Mentel, T. F., and Ehn, M.: Multi-generation OH oxidation as a source for highly oxygenated organic molecules from aromatics, Atmos. Chem. Phys., 20(1), 515–537, doi:10.5194/acp-20-515-2020, 2020.

Guo, S., Hu, M., Zamora, M. L., Peng, J., Shang, D., Zheng, J., Du, Z., Wu, Z., Shao, M., Zeng, L., Molina, M. J., and Zhang, R.: Elucidating severe urban haze formation in China, Proc. Natl. Acad. Sci. USA, 111(49), 17373–17378, doi:10.1073/pnas.1419604111, 2014.

Guo, S., Hu, M., Lin, Y., Gomez-Hernandez, M., Zamora, M. L., Peng, J., Collins, D. R., and Zhang, R.: OH-Initiated Oxidation of m-Xylene on Black Carbon Aging, Environ. Sci. Technol., 50(16), 8605–8612, doi:10.1021/acs.est.6b01272, 2016.

De Haan, D. O., Hawkins, L. N., Kononenko, J. A., Turley, J. J., Corrigan, A. L., and Tolbert, M. A., Jimenez, J. L.: Formation of Nitrogen- Containing Oligomers by Methylglyoxal and Amines in Simulated Evaporating Cloud Droplets, Environ. Sci. Technol., 45, 984− 991, 2011.

De Haan, D. O., Hawkins, L. N., Welsh, H. G., Pednekar, R., Casar, J. R., Pennington, E. A., de Loera, A., Jimenez, N. G., Symons, M. A., Zauscher, M., Pajunoja, A., Caponi, L., Cazaunau, M., Formenti, P., Gratien, A., Pangui, E., and Doussin, J.-F.: Brown Carbon Production in Ammonium- or Amine-Containing Aerosol Particles by Reactive Uptake of Methylglyoxal and

https://doi.org/10.5194/acp-2021-951
Preprint. Discussion started: 15 December 2021

374 Photolytic Cloud Cycling, Environ. Sci. Technol., 51(13), 7458–7466,
375 doi:10.1021/acs.est.7b00159, 2017.

376 Heald, C. L., Jacob, D. J., Park, R. J., Russell, L. M., Huebert, B. J., Seinfeld, J. H., Liao, H., and
377 Weber, R. J.: A Large Organic Aerosol Source in the Free Troposphere Missing from Current
378 Models. Geophys. Res. Lett., 32, 1−4, 2005.

379 Hems, R. F., and Abbatt, J. P. D.: Aqueous Phase Photo-oxidation of Brown Carbon Nitrophenols:
380 Reaction Kinetics, Mechanism, and Evolution of Light Absorption, ACS Earth Sp. Chem., 2(3),
381 225–234, doi:10.1021/acsearthspacechem.7b00123, 2018.

382 Hodzic, A., Kasibhatla, P. S., Jo, D. S., Cappa, C. D., Jimenez, J. L., Madronich, S., and Park, R.
383 J.: Rethinking the Global Secondary Organic Aerosol (SOA) Budget: Stronger Production, Faster
384 Removal, Shorter Lifetime. Atmos. Chem. Phys., 16, 7917−7941, 2016.

385 Hua, W., Jubb, A. M., and Allen, H. C.: Electric Field Reversal of Na2SO4, (NH4)2SO4, and
386 Na2CO3 Relative to CaCl2 and NaCl at the Air/Aqueous Interface Revealed by Heterodyne
387 Detected Phase-Sensitive Sum Frequency, J. Phys. Chem. Lett., 2(20), 2515–2520,
388 doi:10.1021/jz200888t, 2011.

389 Huang, Y., Zhao, R., Charan, S. M., Kenseth, C. M., Zhang, X., and Seinfeld, J. H.: Unified Theory
390 of Vapor–Wall Mass Transport in Teflon-Walled Environmental Chambers, Environ. Sci.
391 Technol., 52(4), 2134–2142, doi:10.1021/acs.est.7b05575, 2018.

392 Intergovernmental Panel on Climate Change (IPCC). *Climate Change 2013: The Physical Science*
393 *Basis. Contribution of Working Group I to the Fifth Assessment Report of the Intergovernmental*
394 *Panel on Climate Change*. Cambridge University Press, 2013.

395 Jenkin, M. E., Saunders, S. M., Wagner, V., and Pilling, M. J.: Protocol for the development of
396 the Master Chemical Mechanism, MCM v3 (Part B): tropospheric degradation of aromatic volatile
397 organic compounds, Atmos. Chem. Phys., 3(1), 181–193, doi:10.5194/acp-3-181-2003, 2003.

398 Ji, Y., Zhao, J., Terazono, H., Misawa, K., Levitt, N. P., Li, Y., Lin, Y., Peng, J., Wang, Y., Duan,
399 L., Pan, B., Zhang, F., Feng, X., An, T., Marrero-Ortiz, W., Secrest, J., Zhang, A. L., Shibuya, K.,
400 Molina, M. J., and Zhang, R.: Reassessing the atmospheric oxidation mechanism of toluene, Proc.
401 Natl. Acad. Sci. USA, 114(31), 8169–8174, doi:10.1073/pnas.1705463114, 2017.

402 Ji, Y., Shi, Q., Li, Y., An, T., Zheng, J., Peng, J., Gao, Y., Chen, J., Li, G., Wang, Y., Zhang, F.,
403 Zhang, A. L., Zhao, J., Molina, M. J., and Zhang, R.: Carbenium ion-mediated oligomerization of
404 methylglyoxal for secondary organic aerosol formation, Proc. Natl. Acad. Sci. USA, 117(24),
405 13294 LP – 13299, doi:10.1073/pnas.1912235117, 2020.

406 Jia, L., and Xu, Y.: Effects of Relative Humidity on Ozone and Secondary Organic Aerosol
407 Formation from the Photooxidation of Benzene and Ethylbenzene, Aerosol Sci. Technol., 48(1),
408 1–12, doi:10.1080/02786826.2013.847269, 2014.

409 Jia, L., and Xu, Y.: Different roles of water in secondary organic aerosol formation from toluene
410 and isoprene, Atmos. Chem. Phys., 18(11), 8137–8154, doi:10.5194/acp-18-8137-2018, 2018.

https://doi.org/10.5194/acp-2021-951
Preprint. Discussion started: 15 December 2021

Atmospheric Chemistry and Physics Discussions

Li, G., Zhang, R., Fan, J., and Tie, X.: Impacts of biogenic emissions on photochemical ozone production in Houston, Texas, J. Geophys. Res., 112, D10309, doi:10.1029/2006JD007924, 2007.

Li, Y., Ji, Y., Zhao, J., Wang, Y., Shi, Q., Peng, J., Wang, Y., Wang, C., Zhang, F., Wang, Y., Seinfeld, J. H., and Zhang, R.: Unexpected Oligomerization of Small α-Dicarbonyls for Secondary Organic Aerosol and Brown Carbon Formation, Environ. Sci. Technol., 55(8), 4430–4439, doi:10.1021/acs.est.0c08066, 2021a.

Li, Y., Zhao, J., Wang, Y., Seinfeld, J. H., and Zhang, R.: Multigeneration Production of Secondary Organic Aerosol from Toluene Photooxidation, Environ. Sci. Technol., 55, 8592−8603, doi:10.1021/acs.est.1c02026, 2021b.

Liu, J., Zhang, F., Xu, W., Sun, Y., Chen, L., Li, S., Ren, J., Hu, B., Wu, H., and Zhang, R.: Hygroscopicity of Organic Aerosols Linked to Formation Mechanisms, Geophys. Res. Lett., 48(4), e2020GL091683, doi:https://doi.org/10.1029/2020GL091683, 2021.

Marrero-Ortiz, W., Hu, M., Du, Z., Ji, Y., Wang, Y. Y., Guo, S., Lin, Y., Gomez-Hermandez, M., Peng, J., Li, Y., Secrest, J., Zamora, M. L., Wang, Y. Y., An, T., and Zhang, R.: Formation and Optical Properties of Brown Carbon from Small α-Dicarbonyls and Amines, , 53(1), 117–126, doi:10.1021/acs.est.8b03995, 2019.

Molina, L. T.: Introductory lecture: air quality in megacities, Faraday Discuss, 226, 9-52, 10.1039/d0fd00123f, 2021.

Moise, T., Flores, J. M., and Rudich, Y.: Optical Properties of Secondary Organic Aerosols and Their Changes by Chemical Processes, Chem. Rev., 115, 4400−4439, 2015.

Molteni, U., Bianchi, F., Klein, F., El Haddad, I., Frege, C., Rossi, M. J., Dommen, J., and Baltensperger, U.: Formation of highly oxygenated organic molecules from aromatic compounds, Atmos. Chem. Phys., 18(3), 1909–1921, doi:10.5194/acp-18-1909-2018, 2018.

National Academies of Sciences Engineering and Medicine (NASEM): The Future of Atmospheric Chemistry Research: Remembering Yesterday, Understanding Today, Anticipating Tomorrow, The National Academies Press, Washington, DC., 2016.

Ng, N. L., Kroll, J. H., Chan, A. W. H., Chhabra, P. S., Flagan, R. C., and Seinfeld, J. H.: Secondary organic aerosol formation from m-xylene, toluene, and benzene, Atmos. Chem. Phys., 7(14), 3909–3922, doi:10.5194/acp-7-3909-2007, 2007.

Nishino, N., Arey, J., and Atkinson, R.: Formation Yields of Glyoxal and Methylglyoxal from the Gas-Phase OH Radical-Initiated Reactions of Toluene, Xylenes, and Trimethylbenzenes as a Function of NO2 Concentration, J. Phys. Chem. A, 114(37), 10140–10147, doi:10.1021/jp105112h, 2010.

Peng, J., Hu, M., Shang, D., Wu, Z., Du, Z., Tan, T., Wang, Y., Zhang, F., and Zhang, R.: Explosive secondary aerosol formation during severe haze in the North China Plain, Environ. Sci. Technol., 55(4), 2189–2207, 2021.

https://doi.org/10.5194/acp-2021-951
Preprint. Discussion started: 15 December 2021

Atmospheric Chemistry and Physics Discussions

Pope, C. A., III, Burnett, R. T., Thun, M. J., Calle, E. E., Krewski, D., Ito, K., and Thurston, G. D.: Lung Cancer, Cardiopulmonary Mortality, and Long-Term Exposure to Fine Particulate Air Pollution. J. Am. Med. Assoc., 287, 1132−1141, 2002.

Ravishankara, A.R.: Heterogeneous and multiphase chemistry in the troposphere, Science 276, 1058-1065, 1997.

Schwantes, R. H., Schilling, K. A., McVay, R. C., Lignell, H., Coggon, M. M., Zhang, X., Wennberg, P. O., and Seinfeld, J. H.: Formation of highly oxygenated low-volatility products from cresol oxidation, Atmos. Chem. Phys., 17(5), 3453–3474, doi:10.5194/acp-17-3453-2017, 2017.

Seinfeld, J. H., and Pandis, S. N.: Atmospheric chemistry and physics: from air pollution to climate change, John Wiley & Sons., 2016.

Shi, Q., Zhang, W., Ji, Y., Wang, J., Qin, D., Chen, J., Gao, Y., Li, G., and An, T.: Enhanced uptake of glyoxal at the acidic nanoparticle interface: implications for secondary organic aerosol formation, Environ. Sci. Nano, 7, 1126−1135, 2020.

Shrivastava, M., Cappa, C. D., Fan, J., Goldstein, A. H., Guenther, A. B., Jimenez, J. L., Kuang, C., Laskin, A., Martin, S. T., Ng, N. L., Petaja, T., Pierce, J. R., Rasch, P. J., Roldin, P., Seinfeld, J. H., Shilling, J., Smith, J. N., Thornton, J. A., Volkamer, R., Wang, J., Worsnop, D. R., Zaveri, R. A., Zelenyuk, A., and Zhang, Q.: Recent advances in understanding secondary organic aerosol: Implications for global climate forcing, Rev. Geophys., 55(2), 509–559, doi:10.1002/2016RG000540, 2017.

Song, C., Na, K., Warren, B., Malloy, Q., and Cocker, D. R.: Secondary Organic Aerosol Formation from m-Xylene in the Absence of NOx, Environ. Sci. Technol., 41(21), 7409–7416, doi:10.1021/es070429r, 2007.

Suh, I., Lei, W., and Zhang, R.: Experimental and theoretical studies of isoprene reaction with NO_3, J. Phys. Chem., 105, 6471-6478, 2001.

Tan, Y., Lim, Y. B., Altieri, K. E., Seitzinger, S. P., and Turpin, B. J.: Mechanisms leading to oligomers and SOA through aqueous photooxidation: insights from OH radical oxidation of acetic acid and methylglyoxal, Atmos. Chem. Phys., 11, 18319−18347, 2012.

Wang, M., Chen, D., Xiao, M., Ye, Q., Stolzenburg, D., Hofbauer, V., Ye, P., Vogel, A. L., Mauldin, R. L., Amorim, A., Baccarini, A., Baumgartner, B., Brilke, S., Dada, L., Dias, A., Duplissy, J., Finkenzeller, H., Garmash, O., He, X.-C., Hoyle, C. R., Kim, C., Kvashnin, A., Lehtipalo, K., Fischer, L., Molteni, U., Petäjä, T., Pospisilova, V., Quéléver, L. L. J., Rissanen, M., Simon, M., Tauber, C., Tomé, A., Wagner, A. C., Weitz, L., Volkamer, R., Winkler, P. M., Kirkby, J., Worsnop, D. R., Kulmala, M., Baltensperger, U., Dommen, J., El-Haddad, I., and Donahue, N. M.: Photo-oxidation of Aromatic Hydrocarbons Produces Low-Volatility Organic Compounds, Environ. Sci. Technol., 54(13), 7911–7921, doi:10.1021/acs.est.0c02100, 2020.

Wennberg, P. O., Bates, K. H., Crounse, J. D., Dodson, L. G., McVay, R. C., Mertens, L. A., Nguyen, T. B., Praske, E., Schwantes, R. H., Smarte, M. D., St Clair, J. M., Teng, A. P., Zhang,

https://doi.org/10.5194/acp-2021-951
Preprint. Discussion started: 15 December 2021

Atmospheric Chemistry and Physics Discussions

X., and Seinfeld, J. H.: Gas-Phase Reactions of Isoprene and Its Major Oxidation Products, Chem. Rev., 118, 3337–3390, 2018.

Xue, H., Khalizov, A. F., Wang, L., Zheng, J., and Zhang, R.: Effects of Coating of Dicarboxylic Acids on the Mass−Mobility Relationship of Soot Particles, Environ. Sci. Technol., 43(8), 2787–2792, doi:10.1021/es803287v, 2009.

Zhang, D., Lei, W., and Zhang, R.: Mechanism of OH formation from ozonolysis of isoprene: Kinetics and product yields, Chem. Phys. Lett. 358, 171-179, 2002.

Zhang, F., Wang, Y., Peng, J., Chen, L., Sun, Y., Duan, L., Ge, X., Li, Y., Zhao, J., Liu, C., Zhang, X., Zhang, G., Pan, Y., Wang, Y., Zhang, A.L., Ji, Y., Wang, G., Hu, M., Molina, M.J., and Zhang, R.: An unexpected catalyst dominates formation and radiative forcing of regional haze, Proc. Natl. Acad. Sci. USA, 117, 3960-3966, doi/10.1073/pnas.1919343117, 2020.

Zhang, Q., Xu, Y., and Jia, L.: Secondary organic aerosol formation from OH-initiated oxidation of m-xylene: effects of relative humidity on yield and chemical composition, Atmos. Chem. Phys., 19(23), 15007–15021, doi:10.5194/acp-19-15007-2019, 2019.

Zhang, R., Wang, L., Khalizov, A. F., Zhao, J., Zheng, J., McGraw, R. L., and Molina, L. T.: Formation of nanoparticles of blue haze enhanced by anthropogenic pollution, Proc. Natl. Acad. Sci. USA, 106, doi:10.1073/pnas.0910125106, 17650-17654, 2009.

Zhang, R., Wang, G., Guo, S., Zamora, M. L., Ying, Q., Lin, Y., Wang, W., Hu, M., and Wang, Y.: Formation of Urban Fine Particulate Matter, Chem. Rev., 115(10), 3803–3855, doi:10.1021/acs.chemrev.5b00067, 2015.

Zhang, R., Johnson, N.M., and Li Y.: Establishing the exposure-outcome relation between airborne particulate matter and children's health, Thorax, 76, doi.org/10.1136/thoraxjnl-2021-217017, 2021.

Zhang, X., Cappa, C. D., Jathar, S. H., McVay, R. C., Ensberg, J. J., Kleeman, M. J., and Seinfeld, J. H.: Influence of Vapor Wall Loss in Laboratory Chambers on Yields of Secondary Organic Aerosol. Proc. Natl. Acad. Sci. U.S.A., 111, 5802−5807, 2014.

Zhao, J., and Zhang, R.: Proton transfer reaction rate constants between hydronium ion (H_3O^+) and volatile organic compounds, Atmos. Environ., 38(14), 2177–2185, doi:https://doi.org/10.1016/j.atmosenv.2004.01.019, 2004.

Zhao, J., Zhang, R., Fortner, E.C., and North, S.W.: Quantification of hydroxycarbonyls from OH-isoprene reactions, J. Am. Chem. Soc., 126, 2686-2687, 2004.

Zhao, J., Zhang, R., Misawa, K., and Shibuya, K.: Experimental product study of the OH-initiated oxidation of m-xylene, J. Photochem. Photobiol. A Chem., 176(1), 199–207, doi:https://doi.org/10.1016/j.jphotochem.2005.07.013, 2005.

Zhu, J., Penner, J. E., Lin, G., Zhou, C., Xu, L., and Zhuang, B.: Mechanism of SOA formation determines magnitude of radiative effects, P. Natl. Acad. Sci. USA, 114, 12685–12690, https://doi.org/10.1073/pnas.1712273114, 2017.

https://doi.org/10.5194/acp-2021-951
Preprint. Discussion started: 15 December 2021

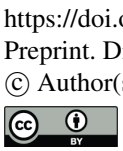

Atmospheric Chemistry and Physics Discussions

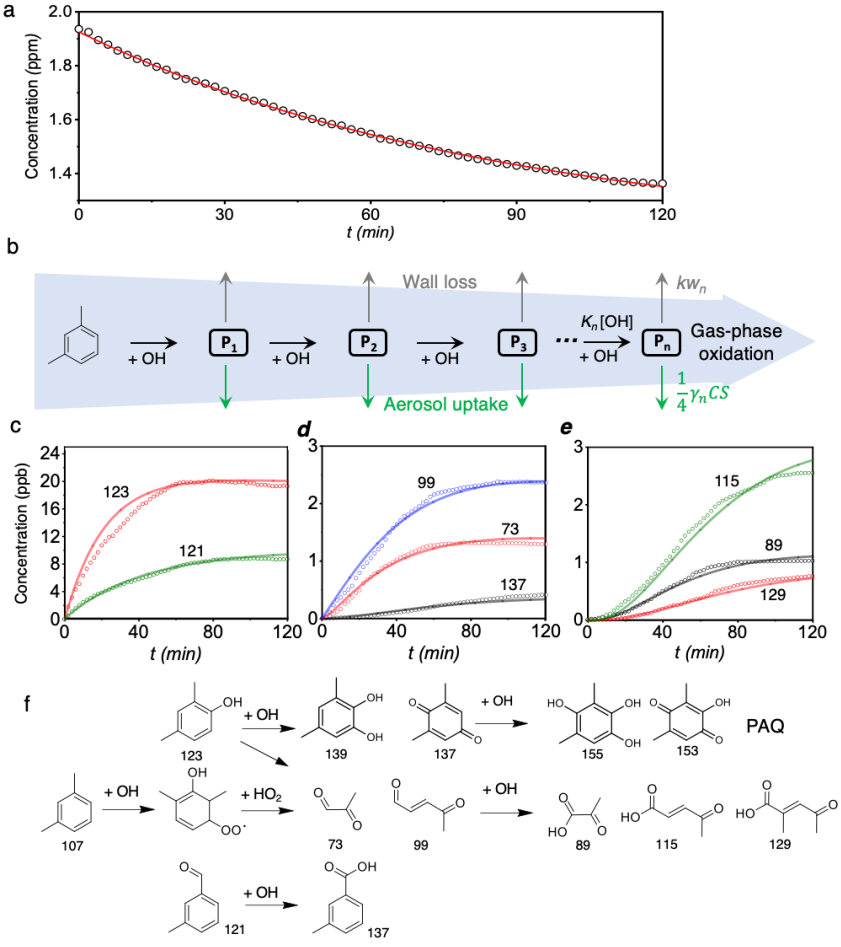

Figure 1. OH-initiated photooxidation of *m*-xylene. (a) Time-dependent concentration of *m*-xylene. The symbols are from the measurements, and the red solid line corresponds to exponential fitting of the *m*-xylene concentration. The initial concentration for *m*-xylene and the estimated steady-state concentration for OH are 1940 ppb and 2.1 × 10^6 molecules cm^{-3}, respectively, with a bimolecular rate constant of 2.4 × 10^{-11} cm^3 $molecule^{-1}$ s^{-1}. (b) Schematic representation leading to the multi-generation product, P_n, where *n* denotes the sequence of OH-initiated oxidation. The black, gray, and green arrows denote the gas-phase oxidation, chamber wall loss, and aerosol uptake, respectively. K_n and kw_n are the rate coefficients for the gas-phase oxidation and wall loss, respectively, γ_n represents the aerosol uptake coefficient, C is the thermal velocity, and S is the aerosol surface area. (c-e) Time-dependent gas-phase concentrations of P_1 (c), P_2 (d), and P_3 (e) products. The symbols are from measurements, and the solid curves are simulated according to the tri-exponential kinetics. (f) The gaseous oxidation pathways leading to the detected products. The top row corresponds to the pathways leading to polyhydroxy aromatics/quinones (PAQ). The numbers in (c) to (f) represents the mass to charge ratio (*m/z*). All experiments are carried out for $(NH_4)_2SO_4$ seed particles with 19 ppb NH_3 at 298 K and RH = 70%. Initiation of photooxidation by ultraviolet light occurs at $t = 0$.

https://doi.org/10.5194/acp-2021-951
Preprint. Discussion started: 15 December 2021

Atmospheric Chemistry and Physics Discussions

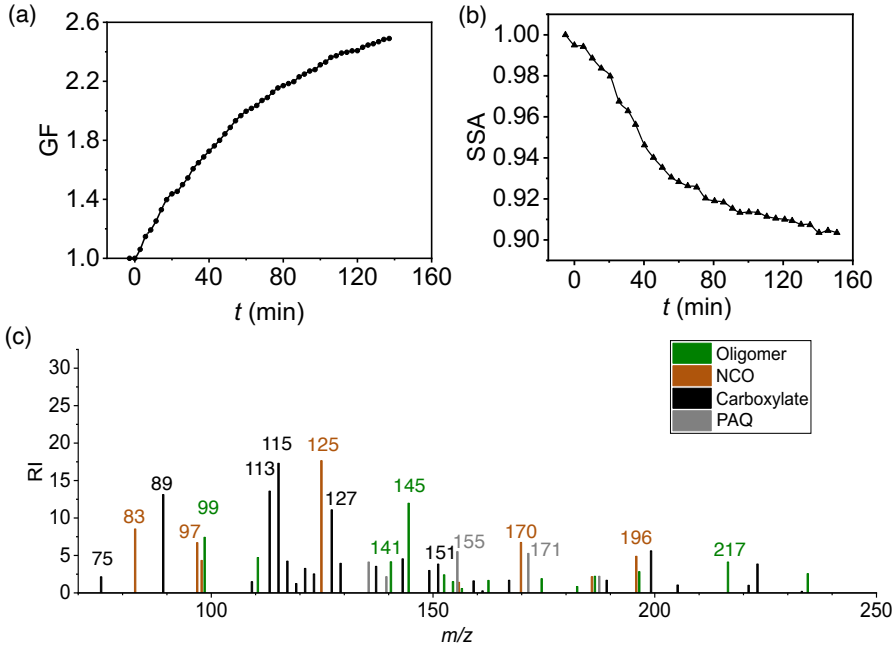

537

538 **Figure 2.** SOA and BrC formation from *m*-xylene photooxidation. Time-dependent growth factor
539 (GF = D_p/D_0, a) and single scattering albedo (SSA, b) of seed particles exposed to *m*-xylene
540 oxidation products. (c) Chemical speciation of aerosol-phase products by TD-ID-CIMS. Initiation
541 of photooxidation by ultraviolet light occurred at t = 0. All experiments are carried out for
542 $(NH_4)_2SO_4$ seed particles with 19 ppb NH_3 at 298 K and RH = 70%.

543

https://doi.org/10.5194/acp-2021-951
Preprint. Discussion started: 15 December 2021

Atmospheric Chemistry and Physics Discussions

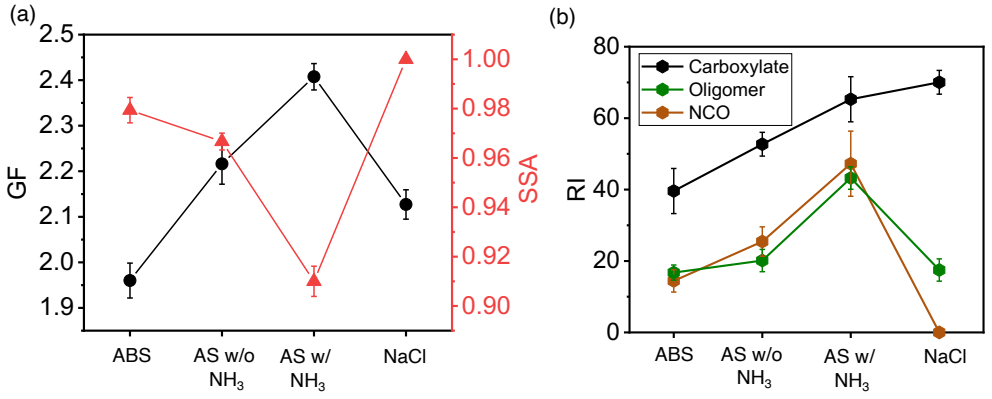

Figure 3. Dependence of SOA/BrC formation on seed particles. (a) GF (black) and SSA (red) at 120 mins of exposure for $(NH_4)_2SO_4$ particles in the presence (AS w/ NH_3) and absence (AS w/o NH_3) of 19 ppb NH_3 and for NH_4HSO_4 (ABS) and NaCl particles in the absence of NH_3. (b) Aerosol-phase relative intensity (RI) for carboxylates (black), oligomers (green), and NCO (brown) on different seed particles. The error bar denotes 1σ of 3 replicated measurements. All particle properties were measured relevant to dry conditions (less than 5% RH) and were dominantly contributed by non-volatile aerosol-phase products.

https://doi.org/10.5194/acp-2021-951
Preprint. Discussion started: 15 December 2021

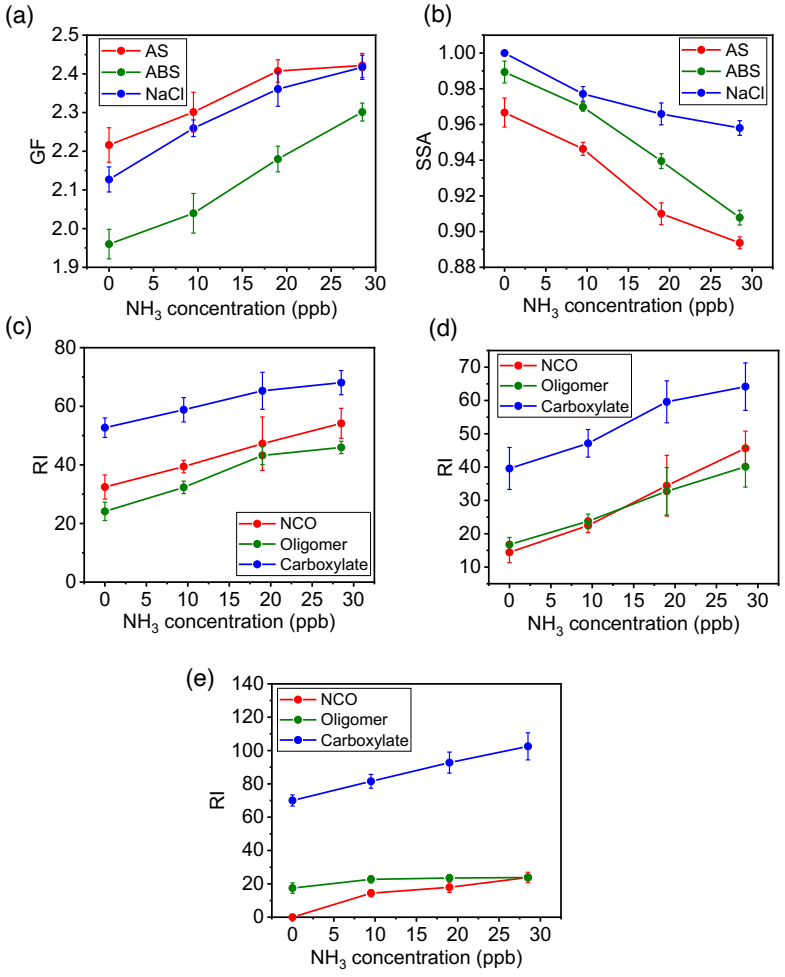

553

554 **Figure 4.** Variation of SOA formation with seed particles and NH_3 concentration. (a,b) growth
555 factor (a) and SSA (b) at t = 120 min with varying NH_3 concentration between 0 and 27 ppb for
556 ammonium sulfate (AS, red), ammonium bisulfate (ABS, green), and sodium chloride (NaCl,
557 blue) seed particles. (c-e) Aerosol-phase mass relative intensity (RI) for NCO (red), oligomers
558 (green), and carboxylates (blue) on AS (c), ABS (d), and NaCl (e) seed particles. The error bar
559 denotes 1σ of 3 replicated measurements.

560

https://doi.org/10.5194/acp-2021-951
Preprint. Discussion started: 15 December 2021

Atmospheric Chemistry and Physics Discussions

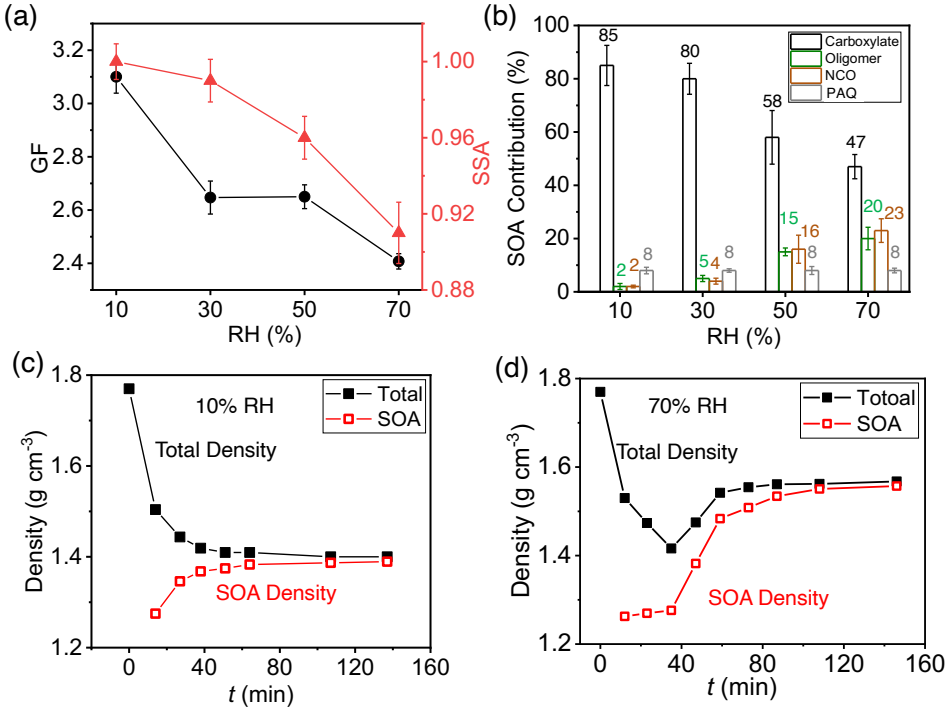

Figure 5. Dependence of SOA/BrC formation on RH. (a) GF (black) and SSA (red) at 120 min with varying RH from 10% to 70%. (b) Contribution of COOs to SOA formation with varying RH from 10% to 70%: carboxylate (black), oligomers (green), NCO (brown), and PAQ (gray) to SOA formation. The number denotes the percentage contribution (%) of each type of aerosol-phase products. (c,d) Time-dependent particle (black) and SOA (red) densities of seed particles exposed to *m*-xylene oxidation products at RH = 10% (c) and 70% (d), respectively. The error bar denotes 1σ of 3 replicated measurements.

https://doi.org/10.5194/acp-2021-951
Preprint. Discussion started: 15 December 2021

Atmospheric Chemistry and Physics Discussions

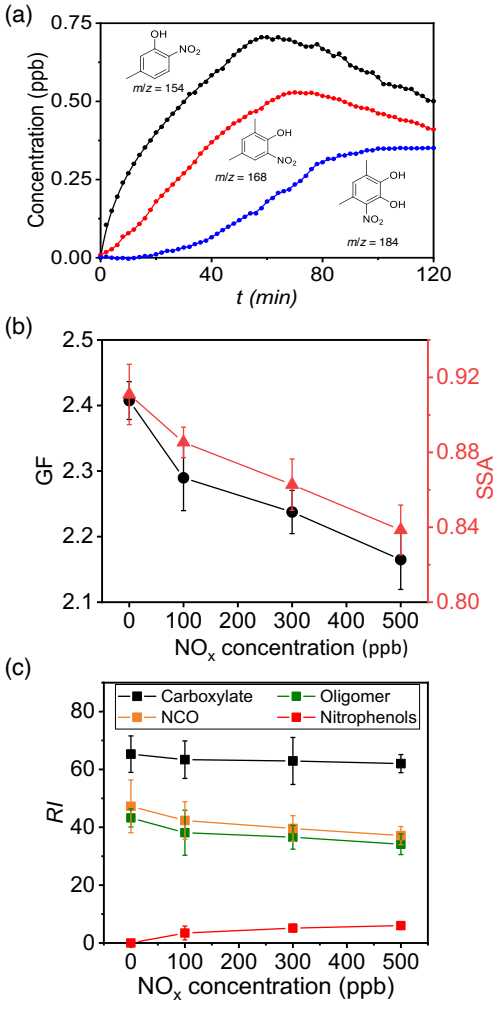

Figure 6. The effects of NO_x. (a) Time-dependent gas-phase concentrations of 5-methyl-2-nitrophenol (black, m/z = 154), dimethyl nitrophenol (red, m/z = 168), and dihydroxy nitrotoluene (blue, m/z = 184). The numbers denote the mass to charge ratio (m/z). Initiation of photooxidation by ultraviolet light occurred at t = 0. (b) GF (black) and SSA (red) at 120 min with varying NO_x concentration from 0 to 500 ppb. (h) Dependence of aerosol-phase relative mass intensities (RI) for carboxylates (black), oligomers (green), NCO (brown), and nitrophenols (red) on NO_x concentration for $(NH_4)_2SO_4$ seed particles with 19 ppb NH_3 at RH = 70%. The error bar denotes 1σ of 3 replicated measurements.

https://doi.org/10.5194/acp-2021-951
Preprint. Discussion started: 15 December 2021

Atmospheric Chemistry and Physics Discussions

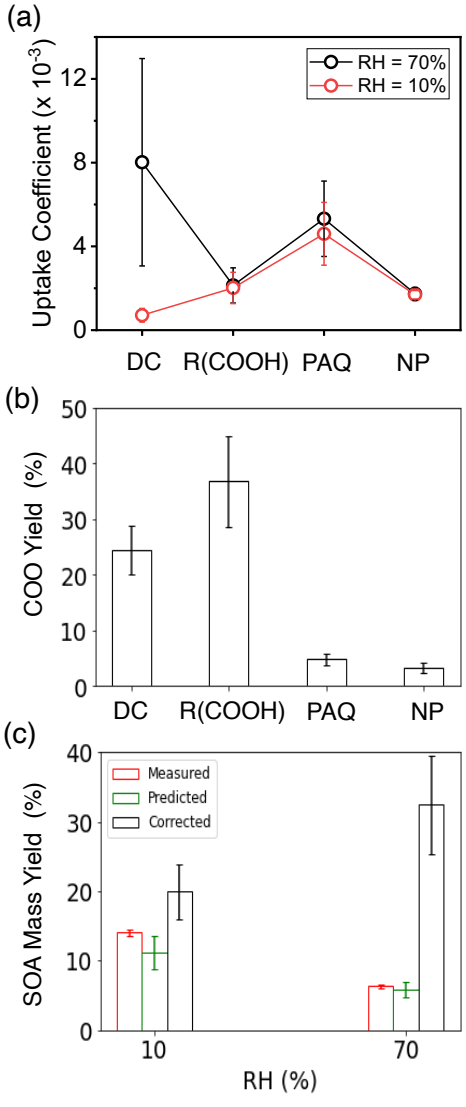

Figure 7. Uptake coefficient, COO yield, and SOA mass yield. (a) Average uptake coefficients (γ) for different types of COOs at 10% (red) and 70% (black) RH for $(NH_4)_2SO_4$ seed particles with 19 ppb NH_3 at 298 K. (b) COO yields: dicarbonyls, organic acids, polyhydroxy aromatics/quinones, and nitrophenols are represented by DC, $R(COOH)_n$, PAQ, and NP, respectively. (c) SOA mass yields at 10% (left columns) and 70% RH (right). The red, green, and black columns represent the measured, predicted, and corrected (for wall loss) SOA mass yields according to eq. 1. All experiments are carried out for 14 μg m^{-3} $(NH_4)_2SO_4$ seed particles with 19 ppb NH_3 at 298 K. The error bars denote the 1σ of 3 replicated measurements or by accounting for error propagation of the measured parameters.